https://doi.org/10.33263/Materials22.219230

ISSN: 2668-5728 https://materials.international

Materials International

Research Article

Volume 2, Issue 2, Pages 0219-0230
2020

Received: 05.03.2020
Accepted: 18.05.2020
Published: 25.05.2020

Heat Pump Thermal Storage for Molton Salt in the Solar Technology

Nima Norouzi [1], Saeed Talebi [2,*], Maryam Fani [3]

[1] Research associate, Energy Department, Amirkabir University of Technology, Tehran, Iran; nima1376@aut.ac.ir
[2] Professor, Energy Department, Amirkabir University of Technology, Tehran, Iran; sa.talebi2015@gmail.com
[3] Professor, Energy Department, Amirkabir University of Technology, Tehran, Iran; mfani@aut.ac.ir
* Correspondence: sa.talebi2015@gmail.com; Scopus ID: 25650802200

Abstract: A thermal heat pump storage technology is based on the Brighton motorcycle transfer from heat transfer from cryogenic thermal storage to the molten solar fluid of salt. The efficiency of long-distance travel, calculated as a function of the turbomachine electrochromic efficiency and heat exchanger steel mass, is competitive with the pumped hydroelectric storage performance. The cost per watt of the engine and the cost of each stored joule are calculated based on current prices for gas turbines and market prices for steel salt and nitrate. A comparison is made with the storage technology of electrochemical and mechanical networks.

Keywords: Energy storage; Solar energy; heat pump, Thermal storage

1. Introduction

It is noticeable that the systems of large scale storage of electricity are essential for any long-term plan to supply fossil fuels with renewable energy [1-3]. It is not precise that the removal of fossil fuels at this time is economically feasible. [4-7] without energy storage, it cannot be useful to its full potential. The urgent demands of customers have shown the crucial importance of timing with the continual development of negative electricity prices in markets with large wind farms.

This paper aims to discuss the specific storage technology and to make the case that in the event of an acute need for storage, eventually, the engineering compromise will be reached. This is a pumped heat storage operation, an idea that is currently being developed in the literature in the industry, and its significant difference with others is the replacement of heat exchangers for thermocouples (Figure 1). Instead of water pumping from a low tank to a smaller tank to store energy, as happens with pumping electricity, one converts thermal energy from a cold object or source to a hot one using an engine. In either case, this trend is reversible so that the energy saved can be harvested later to meet demand.

Heat is added to and removed from the Brayton closed-circuit engine fluid by heat exchangers with anti-current storage fluids. In the basic case, the main fluid is Ar, and the heat-storing source is salt in the molten form (high-pressure) and an organic liquid (a low-pressure). The fluids are stored in 4 tanks at different temperatures restricted by conditions $T + 0 / T0 = T + 1 / T = \xi$. The engine is fully reversible when the turbine-compressor coupling is completely adiabatic, and the heat exchangers are huge. The non-uniformity in the turbomachinery of factories and heat exchangers creates an entropy that must enter the

Cite This Article: Norouzi, N.; Talebi, S.; Fani, M. Heat Pump Thermal Storage for Molton Salt in the Solar Technology. Mat Int 2020, 2, 0219-0230. https://doi.org/10.33263/Materials22.219230

environment as waste heat. This loss leads to the efficiency of the far trip, as shown in Eq. (1)

The argument leading to the "Brayton Battery," as it may be called, applies safety standards, low cost, and high efficiency. The average power delivered to large metropolises such as Los Angeles or New York. Save this power for only one hour to give Hiroshima's 5.01*1013 J or an atomic bomb. The explosive release of this stored energy must be physically impossible. When these safety factors are met, capital and maintenance costs must be brutally minimized, even at the cost of a small blow to travel efficiency, because energy storage is substantially about value, not about saving energy.

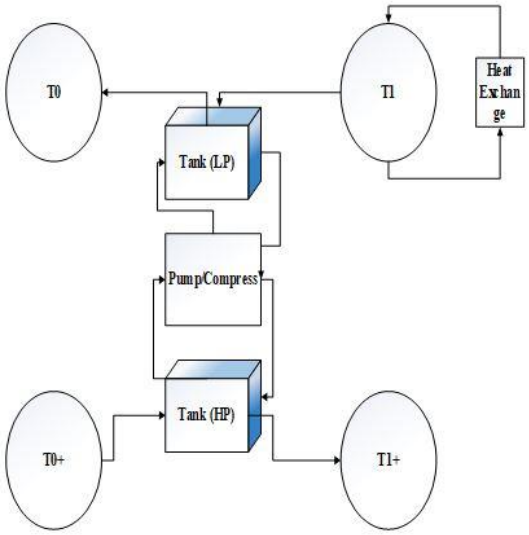

Figure 1. The schematics of the system proposed in this paper (drawn by the authors)

Warehouse storage efficiency meets the primary airflow of configuration in Figure 1.

$$\eta_{store} < \left(1 - \left(\frac{2T_{dump}}{T_1 - T_0}\right)\left(\frac{1}{\eta_c} - \eta_T\right)\left(\frac{\ln(\xi)}{\xi - 1}\right)\right) \quad (1)$$

Where ηc and ηt are the electrochromic efficiency ratio of compressor and turbine, respectively, the Tdump temperature is the temperature at which the waste heat is reduced. For the model of this paper, variables in Table 1, "this limit is 0.75. Factor 2 in Eq. (1), which is caused by the need to pass the working fluid through the [7]" plant turbomachine twice per storage cycle, the performance drawback of hydroelectric or heat pumps is unfortunate.

The design parameters are assumed throughout this paper. The difference between the charge and discharge is ignored for clarity, as the T_{dump} needs to be above the ambient to soften the heat. The multipolar efficiency of the ηc compressor is the ratio of the ideal compression work to the actual compression work at a low compression rate (i.e., for a single step Poly-Ethiopian turbine efficiency, which reverses this ratio to a small extent). These specific values of ηc and ηt are industry standards, which are discussed further in Sec.

Table 1. Design parameters.

Parameter	Argon	Nitrogen
T0	-93.2C	-93.2C
T0'	26.8 C	26.8C
T1	221.8	221.8
T1'	549.8C	549.8C
T_{dump}	26.8 C	26.8C
ξ	1.63	1.63
ηc	0.905	0.905
ηt	0.92	0.92
PO	1 bar	1 bar
pl	10 bar	10 bar
ph	35 bar	7 bar

2. Materials and Methods

2.1. Assumptions and limitations

Brayton Cycle Loss As shown in Figure 1, the fluid pressure of the background work increases, thus reducing the cost per watt of the engine. The rotational speed of the turbine and turbine-blade angles controls the central fluid velocity to approximately the first approximation and, thus, by increasing the pressure, merely increasing the number of working fluid molecules passing at a given point in seconds and thus increasing the total power Give. Background pressures of $7.7*10^6$ Pa (77 atmospheres) compressed to $1.38*10^7$ Pa Experimental in Brayton closed-cycle engines utilizing supercritical Carbon Dioxide [20] pressures near 3.0×10^7 Pa (300 bar) are typical in supercritical vapor are supercritical. Power plants

However, the use of mainly high-pressure restricts the temperature that one can use. As shown in Fig. 2, an increase in the temperature of steel will eventually cause it to creep, resulting in a slow plastic deformation that causes complete mechanical breakdown at more significant temperatures scales. This process is irrelevant on a short-term scale but is an essential constraint on the 40-year-old scale design. [22] Creep is what prevents the use of ordinary carbon steels in high-pressure heat applications at temperatures above 700 K (427 ° C). By adding impurities to the percentages that inhibit grain boundary movement, this limit can be increased to about 800 Kelvin (527 ° C). However, maximum creep resistance requires complete alloying of Cr and Ni to form anti-alloy steels. It has a creep restriction on alloy-steels may be seen from Figure 2 for universal application, including in Inconel. Therefore, pressure vessels made of steel become problematic for temperatures well above 873 Kelvin (600 ° C). This is an essential case in today's supercritical steam plants. [21]

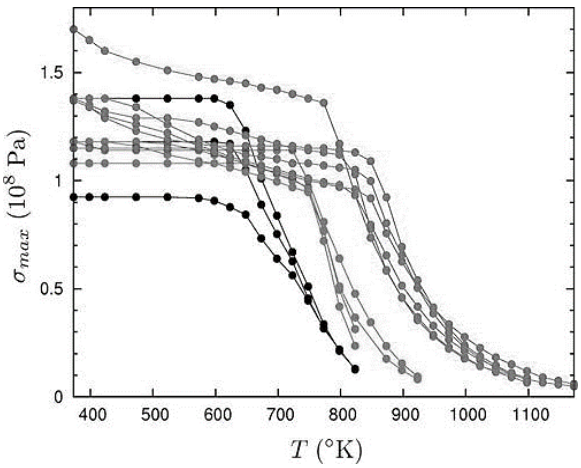

Figure 2. Maximum steel stress permitted by boiler and pressure vessel adapted from ASTM E2860-12 (by the authors).

Part 2, Section 4, Tables 1 and 2 for the selection of steels representative (seamless pipe) .22 "Crawling rock" at T = 873 Kelvin (600 ° C). "It is visible. Black: Carbon steels, UNS K01201, K02707, and K03501. Red: Low alloy steels, UNS K11522, K11547, K11597, and K21590. Blue: Stainless steels, UNS S30409, S30815, S31609, S32109, S34709 and N08810 (Incalloy 800H."

2.2. Molton salt.

The temperature limitation of steels makes solar salt, the $NaNO_3$ / KNO_3 eutectic staple concentrated solar concentrator industry, a good choice for high-temperature storage environments. [23-25] All solids and liquids have an approximate thermal capacity of 3R per mole of the atom, where R is the ideal global gas constant in the suitable temperature range, so almost anything as a thermal storage device, including The rocks act. However, the cost of sand or salt is less than the cost of a thermal heat engine for loads of less than one day. It has the advantage of being very fluid, thus minimizing entropy as a result of the possibility of heat transfer by the anti-processor. Solar Salt has well-known other advantages, including low-pressure steam, high suitability with steels, and environmental friendliness. In response to thermal cycling, it does not emphasize the method of having a solid. It does not cause any explosive hazards.

The $NaNO_3$ / KNO_3 phase diagram illustrated in Fig. 3. Solder Essen. Also, there is a boundary of decomposition for approximately 823 Kelvin (550 ° C), which is easily near the steel creep rock shown in Fig. 1. [29-32] The decomposition boundary is a point where performance is difficult to predict, not where salt begins to fail. The first level of nitrate (NO3) decomposition is reversible and occurs through the nitrate / Nitrate reaction

$$2NO_3 \rightarrow 2NO_2 + O_2$$

Approximately 3% nitrate is converted to nitrite at 823 K (550 ° C). 29 The kinetics of outpatient and O2 reabsorption has been measured and do not appear to be unintentionally rapid. At high temperatures above 923 K (700 ° C) .32 The operating temperature above the solar salt exposed to air is currently unclear. [32] The corrosion of stainless steel by these salts is mild. It is estimated ten micrometers per year at 823 Kelvin (550 ° C), mainly due to oxidation. [33,34]

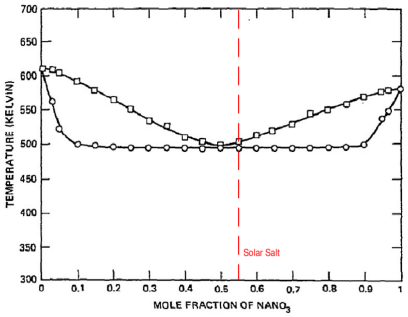

Figure 3. The $NaNO_3$ / KNO_3 phase diagram (by the authors); (The figure was adapted and reused under CC BY license).

Following Rogers and Johns is the measurement of the solid and liquid lines of Rogers and Janes as well as Kramer and Wilson [27]. These lines are due to Zhang et al. [28] The eutectic freezing point is 495 Kelvin (222 ° C). The temperature of decomposition is 550 ° C [29-32].

Figure 4 shows the essential thermal properties of solar salt over a wide range of temperatures.

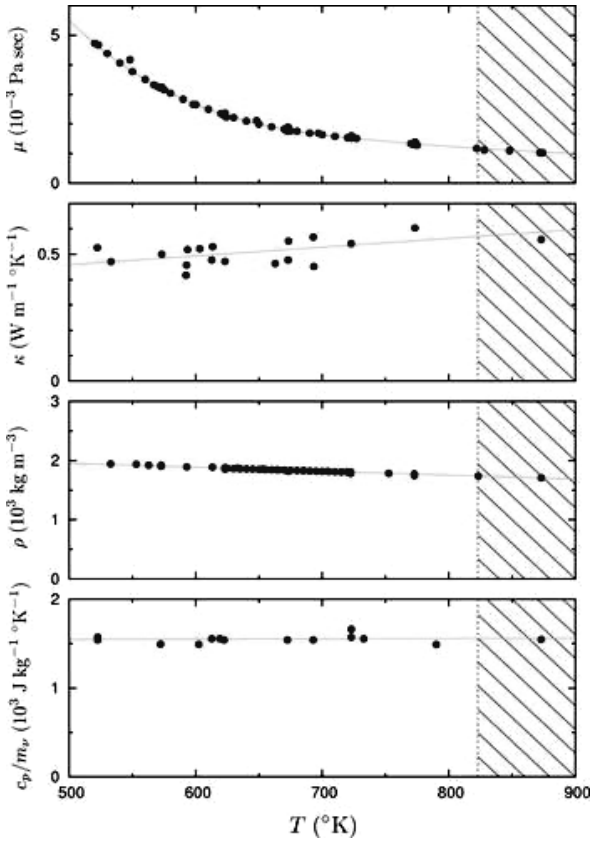

Figure 4. Thermophysical properties of eutectic NaNO3 / KNO3. (by the authors).

The viscosity data are from Johns et al. As provided by Lasfargues et al. The solid line is well suited to Johns et al. At 730 K, it spins a series of power at 1/T. The other data and their interpolation are from Bauer et al. The calorific value of $cp^{ideal}/mv = 15R/mv = 1330\ J.K^{-1}.kg^{-1}$. For comparison, room temperature has $\mu = 0.001$ Pa.s, $\varkappa = 0.59\ W.m^{-1}.K^{-1}$, $\varrho = 1000\ kg.m^{-3}$ 3, and $cp/mv = 4810\ J.kg^{-1}K^{-1}$.

2.3. Working fluid.

The primary fluid in this process is limited to gas elements that are very stable at high temperatures and are not free from liquefaction or solidification phase transfer in mild and idle cases. The mechanical benefits of working near a critical point are outweighed by the risk of fluid or snow falling and damage to the blades. This destroys, in particular, Carbon dioxide, which has a liquidity and freezing transition in the 200-300 kg. The advantages of a low compression pressure ratio and, potentially, higher adiabatic efficiency using an inert gas with no degree of freedom prefer Ar as the superior option. However, the N2 has the advantage of only requiring minor modifications to the airfoil rotor and stator forms previously optimized for use on air-breathing jet engines.

3. Results and Discussion

3.1. Instauration.

The practical material limitations described in Section 2 require T^{+}_{0} smaller than T_1. As illustrated in Fig. 1, these conditions overlap the heat on the high pressure and low-pressure sides of the circuit, thus eliminating the need for heat transfer into or from the fluid stored in this temperature range. It destroys. Instead, heat can simply be transmitted directly from one side of the system to the other sides through a gas heat-exchanger, referred to as a regenerator or retractor. To the extent that the entropy produced by heat exchangers is zero,

reconstruction does not affect travel performance. However, it just reduces the amount of heat-exchanger steel material required [1]. It also reduces the temperature range where stored fluids are needed.

Interpretations clarify why T^{+}_{0} cannot exceed Tdump. A low-pressure Tdump-balanced motor can be easily reset by heating the solar (frozen) salt from Tdump to T1, but if T + 0 is easily reset. It should cool slightly below Tdump.

The calculations justify the selection of T1 as the solar salt melting point. With T^{+}_{1}

Moreover, T^{+}_{0} was fixed at Eq at solar and ambient temperatures, respectively. (1) is Maximized when ξln(ξ /(ξ-1)) to the maximum. However, it can be seen from the diagram of this function in Fig. 8 that at least when $\xi \to 1$ occurs, other costs not computed in this calculation escape to this extent, so the specific value of $\xi = 1$ is significant. Is not. However, the convergence of self-function to 1 is so significant that no efficient round-trip penalty for $1 < \xi < 2$. There is not, in fact, any value of ξ in this range. Besides, lowering the T1 rather than improving it reduces productivity. Therefore, there is no decisive advantage of using special salts at low melting temperatures.

3.2. Round-trip efficiency.

The efficiency of the round-trip storage is simply calculated from the entropy budget. The entropy of the S system must be the same before and after the storage cycle as this property is the case, so any ΔS entropy generated during the cycle must be discarded as the TdumpΔS waste heat, where the Tdump is temperature-dependent, is the environment. This heat represents the loss of stored energy that cannot be transferred back into the grid. So we have the following formulation:

$$\eta_{store} < 1 - \frac{T_{dump}}{T_f} \quad asum.\left(\frac{1}{T_f} = \frac{\Delta S}{E_{store}}\right) \quad (2)$$

The main driving forces of the fictive temperature in the system comes from turbomachines and heat exchangers. Which have been modeled in the following table:

Table 2. Formulation off the round-trip (by the authors)

Phenomena	Formulation
Tf	$\frac{1}{T_f} = \frac{1}{T_f^{Turbo}} + \sum 1/T_f^{ex}$
Turbo Tf	$T_f^{Turbo} = \frac{(T_1 - T_0)(1 - \eta_t\eta_c)(\xi - 1)}{2.\eta_c.\ln(\xi)}$
HE Tf	$T_f^{HE} = \frac{\frac{24\pi\kappa}{11}\left(\frac{T(T_1 - T_0)(\xi - 1)}{\Delta T}\right)^2 \left(s^{in} + s^{out}\right)}{\frac{s^{in}}{L_0^2}}$

The other energy losses in the motors and pressure drops are considered in corrected coefficients.

Table 3. The results of the model for Ar(by the authors)

Ar	Low	Regen.	High
T	233.5 K	392.1 K	649.8 K
ΔT	118 K	189 K	321 K
$p^{(in)}$	10 bar	35 bar	35 bar
$p^{(out)}$	1 bar	1 bar	1 bar
σ_{max}	1.30 × 10^5 kPa	1.30 × 10^5 kPa	1.00 × 10^5 kPa
b/a	1.221	1.221	1.478
d/b	2.43	4.221	2.41
$S\,(out)/S\,(in)$	0.0399	0.6411	0.0231
ℓ	1.69 × 10^−8 m	9.82 × 10^−9 m	1.78 × 10^−8 m
a	0.00132 m	0.00132 m	0.00132 m
$L0$	24.8 m	42.1 m	24.70 m
L	20.00 m	30.00 m	20.00 m
N/E	0.0657 W^−1	0.0421 W^−1	0.0311 W^−1
M/E	0.0355 kg W^−1	0.0362 kg W^−1	0.0424 kg W^−1
T^{hx}_f	30 994 K	34 278 K	32 364 K

Table 4. The results of the model for N2(by the authors)

N2	Low	Regen.	High
T	233.5 K	392.1 K	649.8 K
ΔT	118 K	189 K	321 K
$p^{(in)}$	10 bar	35 bar	35 bar
$p^{(out)}$	1 bar	1 bar	1 bar
σ_{max}	1.30 × 105 kPa	1.30 × 105 kPa	1.00 × 105 kPa
b/a	1.221	1.221	1.478
d/b	2.43	4.989	2.41
$S\,(out)/S\,(in)$	0.059	0.8031	0.0411
ℓ	1.81 × 10−8 m	5.73 × 10−9 m	1.13 × 10−8 m
a	0.00132 m	0.00132 m	0.00132 m
$L0$	35.3 m	102.90 m	62.10 m
L	20.00 m	30.00 m	20.00m
Re	3000.0	3000.0	3000.0
N/E	0.04210 W−1	0.02720 W−1	0.01930 W−1
M/E	0.0228 kg W−1	0.0231 kg W−1	0.0251 kg W−1
T^{hx}_f	33 887 K	39 761 K	44 114 K

3.3. Cost.

The storage cost of the network storage $\mathcal{C}$ has two distinct criteria: the cost per watt motor $\partial\mathcal{C}/\partial$E and the cost per joule stored $\partial\mathcal{C}/\partial$E. It depends on

the energy or the duration. The latter characterizes the storage space and is entirely independent of the rapid transfer of energy into or out. It is thought to put the engine in a specific power category (and cost) first and then add as much storage capacity. It is a raw estimate of the cost per watt of the engine

$$\frac{\partial \mathcal{C}}{\partial \dot{E}} = \frac{\frac{T_{GT}^{ex} - T_{dump}}{(T1 - T0)(\xi - 1)}\left(\frac{\eta_{GT1}}{1-\eta GT}\right)\left(\frac{c_p^{N2}}{c_p}\right)\left(\frac{p0}{pl}\right)\partial \mathcal{C}GT}{\partial \dot{E}} + \frac{2\,\partial \mathcal{C}steel}{\partial M} + \sum ME \quad (3)$$

The description of these variables and their values are summarized in Tables 1 & 4. The basic idea is that the factory turbocharger should cost about the same as today's commercial gas turbine. Therefore, one of the values of today's gasoline turbine measures the number of mol/s, $\dot{v}$ needed to give the given power. The marginal costs of the (immense scale) heat exchangers required are twice the cost of the steel used to manufacture them. This is very unrealistic in today's heat-exchanger market, but that is an expectation for large-scale mass production. This is consistent with the 2 $/kg in heat exchanger price figures studied by Loh et al., Assuming a pipe width of 0.125 times the diameter of the pipe, the ASME standard milling margin.

The parameters used in Eq. (3) To estimate the cost per watt motor $\partial\mathcal{C}/\partial$E; The total fabricated temperature Tf is calculated by Eq. (1) Using the values in Table 4. The total mass per watt motor is calculated by summing the values in Table IV ∑M/E. The exhaust temperature is standard TexGT gas and the thermodynamic efficiency of ηGT from Brooks. The cost of a gas turbine per watt $\partial\mathcal{C}$GT/E engine is black and Veach, as reported by NREL. Black and Veach cost 0.60 $/W for a simple cycle power plant, which agrees with Tidball et al. The price of steel pipes per kilogram Celsius ∂C/∂M is at the very bottom edge of the market range. Fenton announced the price of 0.6 $/kg as steel o carbon. The cost of stainless-steel is typically five times the cost of carbon steel. Bottom: The variables used in Eq. (4) To estimate the marginal cost per joule stored $\partial\mathcal{C}/\partial$E. The cost of eutectic nitrate is per kg of $\partial\mathcal{C}$salt/∂M from Apodaca. The hexane cost per $\partial\mathcal{C}$hex/∂M is the gas price reported by the U.S. EIA.

Table 5. Cost analysis results(by the authors).

	Ar	N2
Tf	1077 K	1098 K
∑M/E	0.1144 kg/W	0.0728 kg/W
TexGT	869 K	818 K
ηGT	36.5%	36.4%
$\partial\mathcal{C}$GT/∂E	0.241 $/W	$0.241 $/W
$\partial\mathcal{C}$steel/∂M	1.02 $/kg	1.02 $/kg
5$\partial\mathcal{C}/\partial$E	0.28 $/W	0.21 $/W
$\partial\mathcal{C}$salt/∂M	0.63 $/kg	0.63 $/kg
$\partial\mathcal{C}$hex/∂M	0.74 $/kg	0.74 $/kg
$\partial\mathcal{C}/\partial$E	3.57 × 10⁻⁶ $/J	$3.58 × 10−6 $/J

A raw estimate of the marginal cost per joule is stored

$$\frac{\partial \mathcal{C}}{\partial E} = \frac{1}{(T_1 - T_0)(\xi - 1)}\left[\frac{\left(\frac{m_{saltv}}{c_{saltp}}\right)\partial \mathcal{C}_{salt}}{\partial M} + \frac{\left(\frac{m_{hexv}}{c_{hexp}}\right)\partial \mathcal{C}_{hex}}{\partial M}\right] \quad (4)$$

Definitions of these variables and their values are presented in Tables 1 & 5. The idea is that the asymptotic cost per joule saved is simply the average cost in which it is stored. In particular, these estimates have been omitted because they are too low for the material, cost of large storage tanks (50 $/m3), and excavators (2.4$/m3).

Equations (3) & (4) are too simplistic, and they involve many obvious costs: flow transfer, cooling structures, tanks, insulation, pumps, site preparation, and accounting for minor damage. However, they are accurate enough to reveal the brush image: The cost of the turbocharger at the Brighton closed-loop plant is reduced to the extent that the cost per watt of the engine is affected by the cost of the heat exchanger. The latter is conceptually unimportant and quickly scaled to arbitrarily large sizes. When they do, they become arbitrarily efficient. Large enough heat exchangers that contribute a negligible share of the total entropy budget can be built for the total cost per watt of a motor comparable to today's simple-cycle gas turbines. The marginal cost per stored joule, which is affected by the cost of storage fluids, is about 3.54*10-6 $/J (12.7 $ per kWh).

The details of the vegetation cost curves of Table 5 in the model calculation are shown by

realizing that these are the only images, given the large error bars, it can be concluded that the storage cost for storage loads is less than one day. So it only matters the cost per watt of the engine and the plant infrastructure. In particular, there is no significant economic advantage in replacing solar and hexane.

Base costs per watt engine $\partial C/\partial E$ engine for Ar and N2 correspond to two solid intercept lines at 0 hours of storage time. The top line is Ar. The range of these lines corresponds to the marginal cost per correspond joule stored $\partial C/\partial E$. The dotted lines show these values with 0.35 $/W added infrastructure cost (cavities, tanks, boards, buildings, etc.), the amount needed to convert a 0.24 $/W gas turbine to 0.6 $/W in a simple cycle.

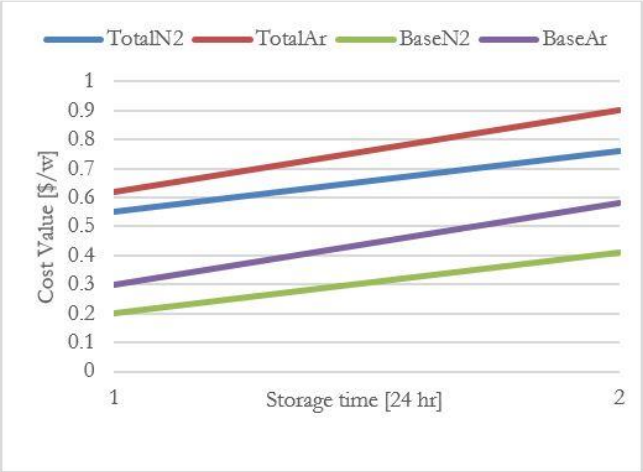

Figure 5. Cost analysis results (by the authors).

3.4. Discussion.

The storage technology that dominates, in the end, depends on its cost, and it is challenging to evaluate it precisely without building machines and testing them. Therefore, it is not possible to create a purely economic case to eliminate the technology described here, which exists only as a concept. Instead, the argument relies in part on a cost analysis that can be done with common sense.

From a physicist's point of view, for example, it makes sense that mechanical components of heat-exchange heat exchangers should be less expensive than the storage of hydroelectric pumps, the technology most associated with them. The turbines are smaller due to faster rotation and faster blade and fluid velocity. They do not need a burner or a razor to cool. Salt and hexane store less energy than water at pump potential: One kilogram of water removed 380 meters, a typical pumping drop, 7.7% of the energy that one kilogram of nitrate salt heats from T1 to $T^{+}1$ Saves, saves. One kilogram of falling water 380 meters transfers 3.4% of the energy to the turbine blades, which cycle 1 kilogram of Ar fluid as it works in the Brayton circuit. In the case of Nitrogen primary fluids, it is 1.73%. Thermal storage also uses less ground than pumped electricity - and of course no mountains or water. This is clearly shown in model calculations, where the footprint of a prototype storage device is plotted based on oil storage tanks. Depending on the construction details, the heat storage requirement maybe 10% or less than the equivalent hydraulic pump storage. Required, calculated from the upper reservoir area.

Its parameters are from Tables 4 and 5. The power is $2.5*10^8$ W. Storage time is 24 hours. The working fluid is Ar. These circles are 14.0 meters long and 30.0 meters radius oil storage tanks. These two collars are for nitrate salts (one for both salt reservoirs in Figures 1 and 3). The remaining four are related to hexane. Heat exchanger units are cylinders 20 m long and 2 m radius, which are hung in parallel. The turbomachine is a very compact plant that is drawn majorly in the figure. However, the gas-turbine, gas-compressor, and the generator are all in the size of a heat-exchanger unit. The energy stored per unit of the footprint is $2.5*10^8$ J/sq.m or approximately 2–10 times the amount of conventional hydroelectric pump storage calculated from the upper reservoir area. It likely stores warm and cold salt in the single tank with a heat insulated barrier in-between them most likely to hexane, so in this manner halving the number of tanks. The entire

facility may also be underground for reasons of heat insulation for the tanks and safety for heat exchangers.

It is also reasonable that heat exchangers should cost just a little more than the steel they are made to manufacture. This is even though large heat exchangers with the specifications of Table 4 are not currently available as products at any cost. Heat exchangers are equivalent to the mechanical engineering of semiconductor memory chips or flat-panel displays: one forces them over and over again millions of times by repeating the same simple step. That means they can be automated. Their production has not been automated yet, but that is because there is no market for such goods. It would be effortless for industrial robots to do this at a little cost.

Batteries had to be used to obtain marginal costs on each of the stored objects from the pumped hydroelectricity, comparing the latter to incorrect. However, they have not done so yet. The issue continues with the construction of new pumping storage facilities around the world.

Two reasons keep the battery charging problem intact. One is that all batteries require a costly internal infrastructure that cannot be removed without shortening and exploding the battery. Energy stored per unit varies from 1.4*105 J/kg for low-cost lead-acid car batteries to 9.5 *10^5 J/kg for high-level lithium-ion batteries. not considerably different from cp/mν(Γ1 - T0)(ξ - 1) = 3.22 × 10^5 J/kg. salt of nitrate, despite the consideration that an active atom in a battery stores ten times more energy than a nitrate salt atom. The extra matter mass is due to atoms that do not store any energy but direct the electron toward the atoms they do. The second is that the battery electrodes are mechanically damaged, especially if the battery is too deep, thus causing long-term maintenance problems. This is because of the surface of the electrode, where the electron moves into ionic motion. The scene of the violence is terrible. Atoms Scale Current batteries and liquid metal batteries reduce collateral damage. However, they do so using engineering compromises that increase other costs. It is unclear whether they are Cheaper than lithium-ion batteries.

Batteries also have environmental issues with their metal ions that lead to forced recycling and prohibition of disposal of household batteries in landfills. This is not the case with heat pumped heat exchange. If the facility shown in the model does not have a catastrophic tank (and fire), the energy stored as harmless heat is lost, and the result is a piece of cold nitrate fertilizer that can be easily cleaned and reuse. If, on the other hand, the current vanadium battery with the same capacity (two tanks required) breaks down, 106 kg of vanadium 8.0*10^6 ions is dumped on the ground with a comparable mass of sulfuric acid.

Therefore, while batteries have the advantage over other forms of small-scale storage over not having a significant input cost per watt motor, this calculation is large enough to prevent cost entry.

Except for hydrogen electrolysis, which has a cost and electrode-like problems with batteries, all other methods for energy storage at the grid-scale have explosive risks at the nuclear scale. This includes, in particular, metal scrap High pressure and all is entirely electric. "Media such as superconductors and superconducting magnetic coils. These media also have lower energy storage density, which is a secondary concern. In the case of steel gates and pressure vessels made of steel, the maximum energy stored per unit matter mass of steel is σmax / ϱsteel or about 2.5% of the thermally stored energy per unit mass of nitrate salt. [25]" For superconductors, this factor is about 10%.

Stored compressed air in underground caves is deliberately removed from the list of explosive technologies. "This is a special case because it is underground (and therefore not explosive) and because it is physically equivalent to heat exchange with heat exchange. It is well known that the energy used to compress any gas is stored in its heat. This is why N2 compression from 1.0 Pa 10^5 Pa to 7.0 × 10^6 Pa (70 atmospheres), the normal underground storage pressure, raises its temperature from 300 K to 1101 K. Putting such hot gas underground is not just for cooling concept. [33]" Therefore, all high-efficiency compressed air storage technologies utilize underground heat exchangers, such as those used in figures 1 & 4 to cool the gas before pumping it underground. Heat is added to the gas during the extraction phase. The physical Variance between underground storage and pure thermal storage with heat-exchange is that "the latter sends the working fluid through the Brighton cycle twice to eliminate the need to store working fluids under pressure and in no way at all. The result of eliminating the need for the cave [22]".

Pumped heat storage with heat exchange is a risk of explosion. This is not the case with heat exchangers with storage media, so it is scaled with

engine power rather than total energy stored. The parameters in Table 3 produce high explosive energy of 90 seconds, which is a design power, whatever that is, for Ar and 166 seconds for N2. Therefore, for the configuration of the model, the explosive power for Ar is 2.20×10^{10} J or 4.8 ton TNT. Heat exchange units of that size and pressure are useful in the petrochemical industry, and they rarely explode, but catastrophic when they do. For example, it does not cascade by sitting underground.

Another serious problem is the costs associated with managing inventory liquids in the event of a breach. Both Ar and N2 have asphaltic gases. They are utterly deadly until they are scattered in the atmosphere. The total inventory of liquids in the model is $2.7*10^5$ kg. Ar. For comparison, the overall amount of CO_2 released in the Lake News disaster is 109 kg.

The heat storage power of the heat pumped pump is controlled by adjusting the working fluid balance up and down by the tremendous heat capacity of the exchanger steel and the slow thermal response related to the regulation of the stored fluid flow in order to keep the temperature constant. The force that the fluid is working on or absorbed by the network is directly proportional to the number of moles passing through a given point in seconds. Since an engine/generator integrated to the grid with other generators is locked in phase by electric forces transmitted through the grid at light speed, the working fluid flow rate is essentially constant, meaning that the person Controls by decreasing or increasing power. Fluid background pressure working in orbit.

Two sets of factory turbochargers may be required, one for storage and the other for extraction. For the parameters of Tables 4 and 5, this increases the cost per watt engine by about $ 0.05 $/W. Unlike the conditions in the pumped power plant, turbomachines cannot be automatically reversed because the blades are airfoils that are carefully manufactured for maximum performance under specific operating conditions, especially for flow and machining speeds. Reversible airfoils can be used for the design, but it is not clear at this time how much work will be required to make the machines work in both directions. The worst-case scenario is which no set of the airfoil will do this properly, which would require two sets of factory turbomachines. As the pressure increases, the cost of a factory turbocharger doubles and decreases.

Table 6. Comparing thermal storage with the other systems of storage(by the authors).

Parameter	Pumped heat storage	Compress air storage	Flywheel storage
Specific Energy	6/10	9/10	10/10
Energy density	6/10	8/10	10/10
Specific power	3/10	5/10	10/10
Efficiency	10/10	10/10	10/10
Lifespan	10/10	10/10	9/10
Cycles	10/10	9/10	10/10
Self discharge	0/10	0/10	10/10
Scale	10/10	9/10	5/10
Energy Capital cost	5/10	5/10	10/10
Power capital cost	10/10	10/10	9/10
Technical maturity	10/10	10/10	10/10
Environmental impact	10/10	10/10	9/10

4. Conclusion

Storage has been a significant concern among energy industry watchers in recent years. As it becomes more urgent that the world moves away from burning fossil fuels, it's also apparent that the intermittency of solar and wind power makes those two sources insufficient substitutes for fossil fuel on their own. With large-scale, cost-effective energy storage solutions, however, it becomes increasingly possible to add more and more renewable energy onto the grid.

Funding

This research received no external funding."

Acknowledgments

In this section, we acknowledge the supports of **Amirkabir University of Technology**.

Conflicts of Interest

The authors declare no conflict of interest.

References

1. Norouzi, N.; Fani, M.; Ziarani, Z.K. The fall of oil Age:A scenario planning approach over the last peak oil of human history by 2040. *Journal of Petroleum Science and Engineering* **2020**, *188*, https://doi.org/10.1016/j.petrol.2019.106827.
2. Kruizenga, A.; Gill, D. Corrosion of Iron Stainless Steels in Molten Nitrate Salt. *Energy Procedia* **2014**, *49*, 878-887, https://doi.org/10.1016/j.egypro.2014.03.095
3. Feldman, D.; Shapiro, M.M.; Banu, D.; Fuks, C.J. Fatty acids and their mixtures as phase-change materials for thermal energy storage. *Solar Energy Materials* **1989**, *18*, 201-216, https://doi.org/10.1016/0165-1633(89)90054-3.
4. Xu, B.; Rathod, D.; Yebi, A.; Onori, S.; Filipi, Z.; Hoffman, M. A comparative analysis of dynamic evaporator models for organic Rankine cycle waste heat recovery systems. *Applied Thermal Engineering* **2020**, *165*, https://doi.org/10.1016/j.applthermaleng.2019.114576.
5. Hasnain, S.M. Review on sustainable thermal energy storage technologies, Part I: heat storage materials and techniques. *Energy Conversion and Management* **1998**, *39*, 1127-1138, https://doi.org/10.1016/S0196-8904(98)00025-9.
6. Hawlader, M.N.A.; Uddin, M.S.; Khin, M.M. Microencapsulated PCM thermal-energy storage system. *Applied Energy* **2003**, *74*, 195-202 https://doi.org/10.1016/S0306-2619(02)00146-0.
7. König-Haagen, A.; Höhlein, S.; Brüggemann, D. Detailed exergetic analysis of a packed bed thermal energy storage unit in combination with an Organic Rankine Cycle. *Applied Thermal Engineering* **2020**, *165*, https://doi.org/10.1016/j.applthermaleng.2019.114583.
8. Flores, R.A.; Aviña Jiménez, H.M.; González, E.P.; González Uribe, L.A. Aerothermodynamic design of 10 kW radial inflow turbine for an organic flashing cycle using low-enthalpy resources. *Journal of Cleaner Production* **2020**, *251*, https://doi.org/10.1016/j.jclepro.2019.119713.
9. Nami, H.; Anvari-Moghaddam, A. Small-scale CCHP systems for waste heat recovery from cement plants: Thermodynamic, sustainability and economic implications. *Energy* **2020**, *192*, https://doi.org/10.1016/j.energy.2019.116634.
10. Yao, Y.; Li, W.; Hu, Y. Modeling and performance investigation on the counter-flow ultrasonic atomization liquid desiccant regenerator. *Applied Thermal Engineering* **2020**, *165*, https://doi.org/10.1016/j.applthermaleng.2019.114573.
11. Saletti, C.; Gambarotta, A.; Morini, M. Development, analysis and application of a predictive controller to a small-scale district heating system. *Applied Thermal Engineering* **2020**, *165*, https://doi.org/10.1016/j.applthermaleng.2019.114558.
12. Nayak, A.k.; Hagishima, A.; Tanimoto, J. A simplified numerical model for evaporative cooling by water spray over roof surfaces. *Applied Thermal Engineering* **2020**, *165*, https://doi.org/10.1016/j.applthermaleng.2019.114514.
13. Chu, S.; Bai, F.; Cui, Z.; Nie, F.; Diao, Y. Experimental investigation on thermal performance of a heat pipe pressurized air receiver. *Applied Thermal Engineering* **2020**, *165*, https://doi.org/10.1016/j.applthermaleng.2019.114551.
14. Oyekale, J.; Heberle, F.; Petrollese, M.; Brüggemann, D.; Cau, G. Thermo-economic evaluation of actively selected siloxane mixtures in a hybrid solar-biomass organic Rankine cycle power plant. *Applied Thermal Engineering* **2020**, *165*, https://doi.org/10.1016/j.applthermaleng.2019.114607.
15. Jung, E.G.; Boo, J.H. Overshoot elimination of the evaporator wall temperature of a loop heat pipe through a bypass line. *Applied Thermal Engineering* **2020**, *165*, https://doi.org/10.1016/j.applthermaleng.2019.114594.
16. Sun, J.; Zhang, G.; Guo, T.; Che, G.; Jiao, K.; Huang, X. Effect of anisotropy in cathode diffusion layers on direct methanol fuel cell. *Applied Thermal Engineering* **2020**, *165*, https://doi.org/10.1016/j.applthermaleng.2019.114589.

17. Norouzi, N.; Kalantari, G.; Talebi, S. Combination of renewable energy in the refinery, with carbon emissions approach. *Biointerface Research in Applied Chemistry* **2020**, *10*, https://doi.org/ 10.33263/BRIAC104.780786.
18. Chen, W.; Huang, C.; Chong, D.; Yan, J. Numerical assessment of ejector performance enhancement by means of combined adjustable-geometry and bypass methods. *Applied Thermal Engineering* **2019**, *149*, 950-959, https://doi.org/10.1016/j.applthermaleng.2018.12.052.
19. Barroso-Maldonado, J.M.; Montañez-Barrera, J.A.; Belman-Flores, J.M.; Aceves, S.M. ANN-based correlation for frictional pressure drop of non-azeotropic mixtures during cryogenic forced boiling. *Applied Thermal Engineering* **2019**, *149*, 492-501, https://doi.org/10.1016/j.applthermaleng.2018.12.082.
20. Saw, L.H.; Poon, H.M.; Chong, W.T.; Wang, C.-T.; Yew, M.C.; Yew, M.K.; Ng, T.C. Numerical modeling of hybrid supercapacitor battery energy storage system for electric vehicles. *Energy Procedia* **2019**, *158*, 2750-2755, https://doi.org/10.1016/j.egypro.2019.02.033.
21. Aly, K.A.; El-Lathy, A.R.; Fouad, M.A. Enhancement of solidification rate of latent heat thermal energy storage using corrugated fins. *Journal of Energy Storage* **2019**, *24*, https://doi.org/10.1016/j.est.2019.100785.
22. Asgharian, H.; Baniasadi, E. A review on modeling and simulation of solar energy storage systems based on phase change materials. *Journal of Energy Storage* **2019**, *21*, 186-201, https://doi.org/10.1016/j.est.2018.11.025.
23. Al Siyabi, I.; Khanna, S.; Mallick, T.; Sundaram, S. An experimental and numerical study on the effect of inclination angle of phase change materials thermal energy storage system. *Journal of Energy Storage* **2019**, *23*, 57-68, https://doi.org/10.1016/j.est.2019.03.010.
24. Li, Z.; Sheikholeslami, M.; Ayani, M.; Shamlooei, M.; Shafee, A.; Waly, M.I.; Tlili, I. Acceleration of solidification process by means of nanoparticles in an energy storage enclosure using numerical approach. *Physica A: Statistical Mechanics and its Applications* **2019**, *524*, 540-552, https://doi.org/10.1016/j.physa.2019.03.129.
25. Seitz, G.; Helmig, R.; Class, H. A numerical modeling study on the influence of porosity changes during thermochemical heat storage. *Applied Energy* **2020**, *259*, https://doi.org/10.1016/j.apenergy.2019.114152.
26. Joybari, M.M.; Seddegh, S.; Wang, X.; Haghighat, F. Experimental investigation of multiple tube heat transfer enhancement in a vertical cylindrical latent heat thermal energy storage system. *Renewable Energy* **2019**, *140*, 234-244, https://doi.org/10.1016/j.renene.2019.03.037.
27. Singh, S.; Sørensen, K.; Condra, T.; Batz, S.S.; Kristensen, K. Investigation on transient performance of a large-scale packed-bed thermal energy storage. *Applied Energy* **2019**, *239*, 1114-1129 https://doi.org/10.1016/j.apenergy.2019.01.260.
28. Cui, G.; Dong, Z.; Wang, S.; Xing, X.; Shan, T.; Li, Z. Effect of the water on the flame characteristics of methane hydrate combustion. *Applied Energy* **2020**, *259*, https://doi.org/10.1016/j.apenergy.2019.114205.
29. Leszczynski, J.S.; Grybos, D. Compensation for the complexity and over-scaling in industrial pneumatic systems by the accumulation and reuse of exhaust air. *Applied Energy* **2019**, *239*, 1130-1141, https://doi.org/10.1016/j.apenergy.2019.02.024.
30. Elsido, C.; Martelli, E.; Kreutz, T. Heat integration and heat recovery steam cycle optimization for a low-carbon lignite/biomass-to-jet fuel demonstration project. *Applied Energy* **2019**, *239*, 1322-1342, https://doi.org/10.1016/j.apenergy.2019.01.221.
31. Yun, S.; Kwon, J.; Cho, W.; Lee, D.; Kim, Y. Performance improvement of hot stamping die for patchwork blank using mixed cooling channel designs with straight and conformal channels. *Applied Thermal Engineering* **2020**, *165*, https://doi.org/10.1016/j.applthermaleng.2019.114562.
32. Yao, Y.; Li, W.; Hu, Y. Modeling and performance investigation on the counter-flow ultrasonic atomization liquid desiccant regenerator. *Applied Thermal Engineering* **2020**, *165*, https://doi.org/10.1016/j.applthermaleng.2019.114573.
33. Norouzi, N.; Talebi, S.; Shahbazi, A. An Overview on the Carbon Capture Technologies with an approach of Green Coal Production study. *Chem. Rev. Lett.* **2020**, 3, https://doi.org/10.22034/crl.2020.224177.1043.
34. Sun, J.; Zhang, G.; Guo, T.; Che, G.; Jiao, K.; Huang, X. Effect of anisotropy in cathode diffusion layers on direct methanol fuel cell. *Applied Thermal Engineering* **2020**, *165*, https://doi.org/10.1016/j.applthermaleng.2019.114589.

35. Norouzi, N.; Talebi, S. xergy and Energy Analysis in Effective Utilization of Carbon Dioxide in the Gas-to-Methanol Process. *Iranian Journal of Hydrogen and Fuel Cell* **2020**, https://doi.org/10.22104/ijhfc.2020.4134.1203.
36. Qin, K.; Li, D.; Huang, C.; Sun, Y.; Wang, J.; Luo, K. Numerical investigation on heat transfer characteristics of Taylor Couette flows operating with CO2. *Applied Thermal Engineering* **2020**, *165*, https://doi.org/10.1016/j.applthermaleng.2019.114570.
37. ASTM E2860-12, Standard Test Method for Residual Stress Measurement by X-Ray Diffraction for Bearing Steels, ASTM International, West Conshohocken, PA, 2012, https://doi.org/10.1520/E2860-12
38. Zhang, X.; Tian, J.; Xu, K.; Gao, Y. Thermodynamic evaluation of phase equilibria in NaNO3-KNO3 system. *Journal of Phase Equilibria* **2003**, *24*, 441-446, https://doi.org/10.1361/105497103770330091.